American Mineralogist, Volume 80, pages 869–872, 1995

Modeling the X-ray diffraction pattern of opal-CT

George D. Guthrie, Jr., David L. Bish
Geology/Geochemistry, Los Alamos National Laboratory, Los Alamos, New Mexico 87545, U.S.A.
Robert C. Reynolds, Jr.
Department of Earth Sciences, Dartmouth College, Hanover, New Hampshire 03755, U.S.A.

Abstract

X-ray diffraction patterns of opal-CT were modeled using a recursive calculation technique that allows for ordered and disordered intergrowths of planar units. The opal-CT structure was modeled as interstratifications of cristobalite and tridymite layers that were based on an idealized trigonal silica sheet, as found in the high-temperature structures. Modeled patterns matched observed patterns well, including the overall shapes of the broad peaks at ~19.5–24.5° 2θ and 35.9° 2θ (Cu$K\alpha$). The calculations allow several important interpretations of opal-CT: XRD patterns of opal-CT can be modeled by an interstratification of cristobalite and tridymite; both disordered and ordered interstratifications occur; particle size can be inferred from the width of the 35.9° 2θ peak; significant information regarding the structural state of opal is contained in weak, often-ignored bands (e.g., one at ~41–46° 2θ); and H_2O is not present in an ordered fashion within the cristobalite and tridymite sheets.

Introduction

Opal is common in many low-temperature environments, and it exists in a number of structural states that are designated opal-A, opal-CT, and opal-C, where A, C, and T signify amorphous, cristobalite, and tridymite, respectively (Jones and Segnit, 1971). During diagenesis, opal matures from opal-A to opal-CT to opal-C (Graetsch, 1994), and this reaction series effectively buffers the activity of silica. Hence, the structural state of opal influences important low-temperature reactions such as illitization and zeolitization.

The effect of opal on silica activity is important in the alteration of tuff, such as occurred at Yucca Mountain, Nevada. Silica activity obviously affected mineral evolution in the zeolitized zones at Yucca Mountain, and it will probably influence future reactions involving zeolites. Because zeolites and reactions involving zeolites play an important role in the migration of radionuclides and because opal can influence zeolite reactions, it is essential to understand the nature of opal in these tuffs. Furthermore, reactions involving opal and other silica polymorphs (e.g., cristobalite) can affect the structural integrity of the tuff because they typically involve changes in the volume of the solids. The structural state of opal is one of the principal factors that influences opal's role in these processes.

Opal-CT has long been recognized as being structurally similar to cristobalite and tridymite (Jones et al., 1964, 1966). Early inferences were based on a qualitative interpretation of X-ray diffraction (XRD) patterns, which typically show a broad band at ~19.5–24.5° 2θ and a broad peak at ~35.9° 2θ (Cu$K\alpha$). At least as early as 1955 (Flörke, 1955, in Jones and Segnit, 1971), it was recognized that this diffraction pattern is consistent with cristobalite that contains stacking disorder, i.e., interstratified cristobalite and tridymite. Several recent studies offer support for this interpretation (Rice and Elzea, 1993; Cady and Wenk, 1994; Graetsch et al., 1994). Rice and Elzea (1993) found that high-resolution transmission electron microscopy (HRTEM) images of opal-CT are consistent with interstratified cristobalite and tridymite layers within particles that range in size from 12 to 32 nm. Cady and Wenk (1994) also reported HRTEM images of several opal samples showing interstratification of cristobalite and tridymite layers. On the basis of data from XRD, nuclear magnetic resonance (NMR), and thermal analysis, Graetsch et al. (1994) concluded that opal consists of cristobalite-tridymite interstratifications. De Jong et al. (1987) also used XRD and NMR to evaluate short- and long-range ordering in opal, but they concluded that opal does not consist of cristobalite and tridymite microcrystallites because the NMR spectra of opal are not simply a superposition of the spectra from cristobalite and tridymite. They favored an interpretation in which the O array first develops long-range ordering followed by the long-range ordering of Si, with the net result that long-range ordering (overall) develops before short-range ordering.

Powder X-ray diffraction remains the most commonly used technique to investigate opal, yet interpretations of opal XRD patterns remain largely qualitative. A detailed interpretation (by modeling) of the opal XRD patterns has the potential to provide solutions to several outstand-

0003–004X/95/0708–0869$02.00

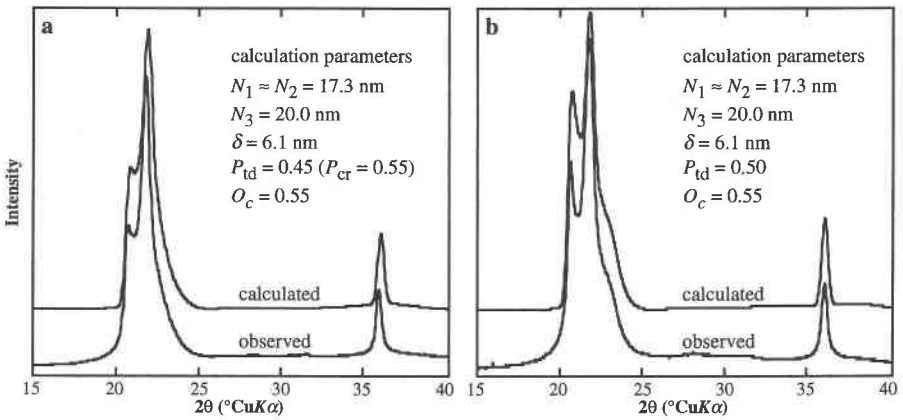

Fig. 1. Comparison of calculated and observed patterns for two opals. (**a**) Calculated for 45% tridymite and random stacking ($O_c = P_{cr}$); observed pattern from 46E5880. (**b**) Calculated for 50% tridymite and 10% ordering ($O_c > P_{td}$); observed pattern from 28501. Note shoulder on high-angle side of 20–25° 2θ band in **b**. Ordering state of the cristobalite-tridymite interstratification can be evaluated by the relationship among O_c, P_{td}, and P_{cr} for the following two cases: for $P_{td} \geq 0.5$, $O_c = P_{td}$ for random interstratification, $O_c > P_{td}$ for ordered interstratification (e.g., $O_c = 1$ produces R1 ordering), and $O_c < P_{td}$ for segregation (e.g., $O_c = 0$ produces complete segregation of cristobalite and tridymite layers); for $P_{td} < 0.5$, $O_c = P_{cr}$ for random interstratification, $O_c > P_{cr}$ for ordered interstratification, and $O_c < P_{cr}$ for segregation. The two cases result from the way in which the junction probabilities are defined. More detailed discussions of probabilities and interstratification are found in Reynolds (1980, 1993).

ing problems. First, modeling can provide support for the hypothesis that opal is an interstratification of cristobalite and tridymite and can provide constraints on the range of structural states found in opal. Second, by modeling the diffraction patterns for suites of different opal samples representing likely diagenetic sequences, one can identify appropriate methods for monitoring the maturation of opal. The current approach to monitoring opal maturation uses the position of the ~21.7° peak (typically reported as d_{101}), which migrates from 0.412 to 0.404 nm during diagenesis (Murata and Nakata, 1974). Modeling may reveal the reason for this peak shift. Finally, results from modeling the diffraction pattern for a particular opal can be used in conjunction with Rietveld methods to determine quantitative mineral abundances.

We have modeled the opal diffraction pattern as an interstratification of cristobalite and tridymite. Our modeling approach allows the variation of particle size, proportions of the two different layers, and ordering state (from segregated layers to disordered interstratifications to R1-ordered interstratifications, where complete R1 ordering refers to a rigorous alternation of the two layer types). Graetsch et al. (1994) attempted to model the diffraction pattern of opal-CT using a simulation program by Treacy et al. (1991). They calculated images for several proportions of tridymite and cristobalite layers (which they referred to as representing "various degrees of stacking disorder"); however, they apparently did not consider R1 ordering as a parameter in their calculations. In other words, their "ordering" refers to the relative probabilities of the two types of layers and not to an ordered interstratification. In this paper, we present our modeling results in detail and show that they can be used to address many of the problems outlined above. We also compare our modeling results with the XRD patterns of several natural opal samples to demonstrate the success of the model and to illustrate the likely ranges in structural states.

Methods

Diffraction patterns were calculated using a modified version of the program Wildfire (R. C. Reynolds, Hanover, New Hampshire), which has been applied successfully to the modeling of three-dimensional XRD patterns of interstratified clays. The details of the computational method used by Wildfire are discussed by Reynolds (1980, 1993). In short, Wildfire simulates the XRD patterns of interstratified layer structures by calculating the Fourier transform of individual layers and by assembling the intergrowth structure in reciprocal space. The contribution from each layer is summed statistically to form the reciprocal lattice of a "virtual crystal" that is representative of a distribution of crystals with various proportions of each layer type and various ordering states and crystallite sizes. In our opal calculations, the variables included the following: probability of tridymite (P_{td}), probability of cristobalite ($P_{cr} = 1 - P_{td}$), maximum crystallite size along the stacking direction **c** (N_3), mean value of the crystallite size along **c** (δ), crystallite size along **a** (N_1) and **b** (N_2), and ordering coefficient (O_c). The significance of the ordering coefficient is described in the Figure 1 caption. Calculations were performed for $\lambda = 0.15418$ nm (i.e., to simulate Cu$K\alpha$ radiation).

The structure of the layer used in our calculations is an idealized sheet, as found in the high-temperature structures of cristobalite and tridymite. The dimensions of the sheet were adjusted so that the positions of the calculated peaks matched those observed. Tridymite stacking was

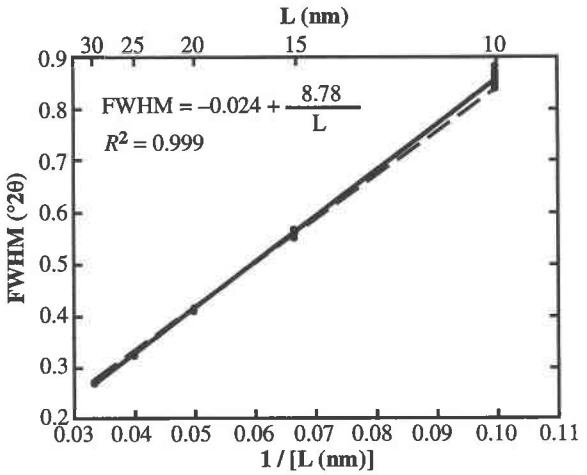

Fig. 2. Relationship between crystallite size (L) and calculated FWHM of the 35.9° 2θ peak. FWHM values taken from patterns calculated over the range in O_c (0.35–0.75) and P_{td} (0.35–0.55) that is larger than the range we generally found for opal-CT. Crystallite size refers to the size along **a** or **b**. Equation in upper left represents a linear regression of FWHM to 1/L with units of degrees two-theta and nanometers. Equation does not take into account instrumental broadening effects; hence, observed FWHM values must be corrected for these effects before being used in this equation. For comparison with the Scherrer equation, we also fit the data using no intercept value and using units of radians and ångströms, which resulted in a K value of 0.907.

modeled as a 180° rotation of successive sheets, and cristobalite stacking was modeled as a shift of successive layers by $a/3$.

Diffraction patterns for opal were collected on a Siemens D500 using Cu$K\alpha$ radiation and a Peltier-cooled SiLi detector. Incident- and diffracted-beam Soller slits were also used during data collection. Scans were generally conducted at the rate of 2 s/0.04° 2θ step, but several longer experiments were collected at rates of 600 s/0.04° 2θ step. Samples were ground under acetone for 10 min in a Brinkmann automated grinder and mounted in front-packed mounts large enough to contain fully the beam at low angles. The full-width half-maximum (FWHM) values for the 35.9° 2θ peak were determined using profile fitting (DIFFRAC5000, v. 2.32; Siemens) and a Pearson-VII profile function.

Observations

Figure 1 exemplifies the success of the model. The dominant features of the opal-CT XRD patterns are reproduced extremely well, including the shapes, positions, and widths of the 19.5–24.5° 2θ band and the 35.9° 2θ peak. The largest discrepancy between the calculated and observed patterns occurs at the low-2θ side of the 19.5–24.5° 2θ band, where the model predicts a sharper peak profile than is observed. To evaluate the uniqueness of our fits, we calculated over 275 patterns covering an extremely large range of model parameters, and the general parameter space consistent with observed patterns is relatively limited.

Table 1. Crystallite size (L) and d_{101} of several opal-CT samples

Sample	FWHM* (° 2θ)	L (nm)	d_{101} (nm)
46E5885	0.777	11.0	0.411
72-300-4	0.627	13.5	0.411
92509	0.567	14.9	0.411
46E5880	0.495	16.9	0.411
28271	0.408	20.3	0.410
28281	0.408	20.3	0.410
28501	0.400	20.7	0.410
47051	0.399	20.8	0.409
114874	0.368	22.4	0.410
28781	0.367	22.5	0.411

Note: 46E5880 and 46E5885 were obtained from Ward's Scientific; 114874 was obtained from the Smithsonian Institute, Department of Mineral Sciences; all other samples were obtained from the Harvard Mineralogical Museum. Localities for the samples are as follows: 46E5885, Virgin Valley, Humboldt County, Nevada; 72-300-4, Somar Company; 92509, Hardtrigger Creek, Owyhee County, Idaho; 46E5880, Jalisco, Mexico; 28271, Kosemnitz, Silesia, former Czechoslovakia; 28281, Steinheim, Germany; 47051, Saint Just, Cornwall, U.K. (also listed as no. 83218); 28501, Kliwikerthal, near Schemnitz, now Banska Stiavnica, former Czechoslovakia; 114874, Red Lake, Albine County, California; 28781, Iceland.

* Full-width half-maximum value of the peak at ~35.9° 2θ was corrected for instrumental broadening effects.

The model allows several important conclusions to be drawn from the observed patterns for opal. First, XRD patterns of opal-CT are consistent with interstratifications of cristobalite and tridymite. This confirms many previous interpretations but apparently conflicts with the interpretations of de Jong et al. (1987), who observed that NMR spectra of opal-CT cannot be reproduced by a superposition of the spectra from cristobalite and tridymite. The fact that our model assumes that cristobalite and tridymite are interstratified on a layer-by-layer basis may resolve this conflict.

Second, the FWHM of the 35.9° 2θ peak is primarily sensitive to the size of the opal crystallites in the **a**-**b** plane. Figure 2 shows the degree of correlation between crystallite size and FWHM for patterns calculated over a large range of structural parameters. The equation in Figure 2 can be used to estimate crystallite size in observed opals, which we have done with XRD patterns of several very pure opal samples (Table 1). The range for the opal crystallite sizes, 11–23 nm, is in excellent agreement with the range of crystallite sizes determined on different opal-CT samples using TEM, 12–32 nm (Rice and Elzea, 1993). Furthermore, the crystallite size increases with increasing opal-CT maturity as estimated by d_{101}, as might be expected.

Third, the 19.5–24.5° 2θ band is sensitive to the relative proportions of tridymite and cristobalite layers. In the samples we investigated by modeling, the amount of tridymite is generally in the range 35–55%, broadly consistent with the results reported by Graetsch et al. (1994). Although the relative intensity of the 20.7° 2θ peak roughly indicates the amount of tridymite (a larger peak indicates more tridymite), the peak is sensitive to several oth-

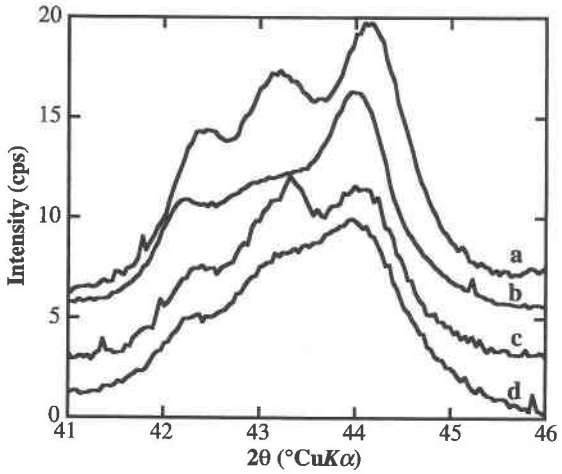

Fig. 3. Observed patterns for various opals, showing the weak intensity band in the 41–46° 2θ region. (a) 28501; (b) 28781; (c) 114874; and (d) 46E5880. Step size was 0.04° 2θ, and counting time was 600 s/step.

er factors (e.g., particle size and ordering state), so the amount of tridymite is best determined by modeling the entire diffraction pattern.

Fourth, the XRD patterns for some opal-CT samples contain a slight shoulder on the high-2θ side of the 19.5–24.5° 2θ band. Within the constraints imposed by other parts of the diffraction pattern (e.g., crystallite size and probability of tridymite), these shoulders were modeled only by introducing a small degree of ordered stacking (Fig. 1b). Large degrees of ordering resulted in the formation of a discrete peak on the high-angle side of the band, which we have not observed in any of our natural opal-CTs.

Fifth, the calculated patterns suggest that several low-intensity diffraction bands, which are not typically investigated in studies of opal, may provide important clues to ordering state. The most intense of these is the band at ~41–45° 2θ. The calculated patterns suggest that the details of this band are very sensitive to ordering (e.g., a peak develops at ~43° 2θ upon ordering). Observed patterns (Fig. 3) exhibit complexities that are consistent with these observations. We are currently investigating the details of this band. Interestingly, two of the samples we have studied thus far (nos. 28501 and 114874) show large particle sizes and indications of ordering (a shoulder on the 19.5–24.5° 2θ peak and a peak at ~43° 2θ) (cf. Table 1 and Figs. 1b, 3a, and 3c). In contrast, sample no. 28781, which also exhibits a large particle size, shows no evidence of ordering (i.e., no shoulder and no 43° 2θ peak) (cf. Table 1 and Fig. 3b). Thus, maturation processes in opal-CT, which include crystallite growth and ordering, do not appear to occur identically in every sample.

Finally, we calculated XRD patterns for opals containing H_2O molecules (with large displacement parameters) in the centers of each of the hexagonal cavities within the silica sheets, and these patterns contained discrete peaks that are not observed in experimental patterns of opal-CT. Hence, H_2O in opal is probably not present on a specific crystallographic site within the opal structure. Rather, the H_2O may occupy a position in the opal structure different from the one we modeled, or it may be located along the boundaries between the 10–35 nm grains.

Acknowledgments

We thank Carl Francis (Harvard Mineralogical Museum), Jeff Post (Smithsonian Institute, Department of Mineral Sciences), and Dave Vaniman (Los Alamos National Laboratory) for providing research samples. We also thank Bill Carey, Sherry Cady, Jessica Elzea, and Peter Heaney for critical reviews of the manuscript and Steve Chipera for help on sample preparation. This work was supported and managed by the U.S. Department of Energy, Yucca Mountain Site Characterization Office. The Los Alamos data tracking number for this work is LA-000000000122.001. The record package containing traceability information is LA-EES-1-TIP-95-001.

References cited

Cady, S.L., and Wenk, H.-R. (1994) Diagenetic microcrystalline opal varieties from the Monterey Formation, CA: HRTEM study of structures and phase transformation mechanisms. Geological Society of America Abstracts with Programs, 26, A112.

de Jong, B.H.W.S., van Hoek, J., Veeman, W.S., and Manson, D.V. (1987) X-ray diffraction and ^{29}Si magic-angle-spinning NMR of opals: Incoherent long- and short-range order in opal-CT. American Mineralogist, 72, 1195–1203.

Flörke, O.W. (1955) Zur frage des "Hoch"—Cristobalit in Opalen, Bentoniten und Gläsern. Neues Jahrbuch für Mineralogie Monatschefte, 217–233.

Graetsch, H. (1994) Structural characteristics of opaline and microcrystalline silica minerals. In Mineralogical Society of America Reviews in Mineralogy, 29, 209–232.

Graetsch, H., Gies, H., and Topalović, I. (1994) NMR, XRD and IR study on microcrystalline opal. Physics and Chemistry of Minerals, 21, 166–175.

Jones, J.B., and Segnit, E.R. (1971) The nature of opal: I. Nomenclature and constituent phases. Journal of the Geological Society of Australia, 18, 57–68.

Jones, J.B., Sanders, J.V., and Segnit, E.R. (1964) Structure of opal. Nature, 204, 990–991.

Jones, J.B., Biddle, J., and Segnit, E.R. (1966) Opal genesis. Nature, 210, 1353–1354.

Murata, K.J., and Nakata, J.K. (1974) Cristobalite stage in the diagenesis of diatomaceous shale. Science, 184, 567–568.

Reynolds, R.C., Jr. (1980) Interstratified clay minerals. In G.W. Brindley and G. Brown, Eds., Crystal structures of clay minerals and their X-ray identification, monograph 5, p. 249–303. Mineralogical Society, London.

——— (1993) Three-dimensional X-ray powder diffraction from disordered illite: Simulation and interpretation of the diffraction patterns. In R.C. Reynolds, Jr. and J.R. Walker, Eds., Computer applications to X-ray powder diffraction analysis of clay minerals, vol. 5, p. 43–78. Clay Minerals Society, Boulder, Colorado.

Rice, S.B., and Elzea, J.M. (1993) Stacking disorder in the crystalline opals. Clay Minerals Society Annual Meeting Abstracts with Program, 137.

Treacy, M.M.J., Newsam, J.M., and Deem, M.W. (1991) A general recursion method for calculating diffracted intensities from crystals containing planar faults. Proceedings of the Royal Society of London, 433A, 499–520.

Manuscript received March 24, 1995
Manuscript accepted June 9, 1995